JACS
JOURNAL OF THE AMERICAN CHEMICAL SOCIETY

ARTICLE

pubs.acs.org/JACS

Quantum Phase Transition from Superparamagnetic to Quantum Superparamagnetic State in Ultrasmall $Cd_{1-x}Cr(II)_xSe$ Quantum Dots?

Weiwei Zheng,[§] Pushpendra Kumar,[†,‡] Aaron Washington,[§] Zhenxing Wang,[§] Naresh S. Dalal,[§] Geoffrey F. Strouse,[§] and Kedar Singh*[,†]

[§]Department of Chemistry and Biochemistry, Florida State University, Tallahassee, Florida 32306-4390, United States

[†]Department of Physics, Faculty of Science, Banaras Hindu University, Varanasi 221005, India

[‡]Nanotechnology Application Centre, Faculty of Science, University of Allahabad, Allahabad 211002, India

Supporting Information

ABSTRACT: Despite a long history of success in formation of transition-metal-doped quantum dots (QDs), the origin of magnetism in diluted magnetic semiconductors (DMSs) is yet a controversial issue. Cr(II)-doped II−VI DMSs are half-metallic, resulting in high-temperature ferromagnetism. The magnetic properties reflect a strong p−d exchange interaction between the spin-up Cr(II) t_{2g} level and the Se 4p. In this study, ultrasmall (∼3.1 nm) Cr(II)-doped CdSe DMSQDs are shown to exhibit room-temperature ferromagnetism, as expected from theoretical arguments. Surprisingly, a low-temperature phase transition is observed at 20 K that is believed to reflect the onset of long-range ordering of the single-domain DMSQD.

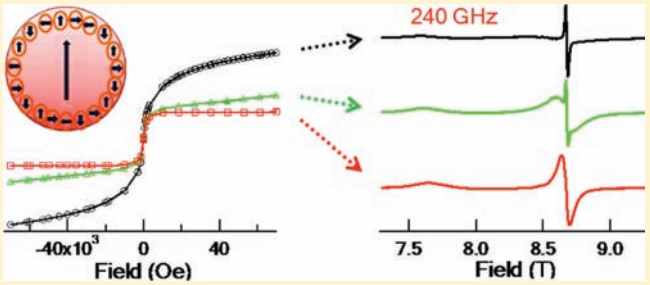

1. INTRODUCTION

Highly monodispersed II−VI[1−4] and III−V[5−7] quantum dots (QDs) have been prepared and applied to various applications, such as light-emitting diodes,[8,9] biological labels,[10,11] and solar cells.[12] During the past decade much effort has been dedicated to preparing quantum-confined semiconductor nanocrystals or QDs that exhibit a large surface-to-volume ratio, size-dependent optical properties arising from the spherical confinement of the electron−hole wave function. The physical size of the QD determines the degree of confinement; therefore, changing the size of the QDs shifts the energy levels.[1] Doping of semiconductor nanocrystals by paramagnetic transition-metal (TM) ions has also attracted attention to size-confinement shifts in the energy levels, which can impact the orbital exchange interactions between the d-levels of the dopant and the valence (p-level) and conduction (s-level).[13,14] The systematic control offered by size tuning endows diluted magnetic semiconductor QDs (DMSQDs) with potential for nanoscale spintronic applications.

Applications based on DMS devices have shown that the efficiency of spin injection from a ferromagnetic metal to an inorganic semiconductor at room temperature can be rather poor,[15] mainly attributed to the conductivity mismatch at the interface between the ferromagnet and the semiconductor.[16,17] In order to overcome this practical difficulty, one needs a semiconductor that is ferromagnetic as a spin-polarized electron source.[18] Both experimental and theoretical works on DMSs with ferromagnetism (FM) have been reported, in particular, for a few 3d TMs, such as Cu, Co, V, Cr, Mn, Fe, and Ni-doped wide-gap semiconductors, such as TiO_2, ZnO, and SnO_2.[19−28] Among these, Cr doping is particularly interesting and has attracted great attention due to the potential for room-temperature FM.[29−33] The most prominent difference between Cr(II)-based DMS materials is the presence of a half-metallic state due to the spin-up and spin-down levels in Cr(II) existing at the Fermi level, which leads to efficient ferromagnetic p−d exchange (β) between the Se (4p) valence-band electrons and the 3d-levels for the Cr(II) ions.[34] The formation of a ferromagnetic DMSQD from Cr(II) doping leads to speculation of the potential for a quantum critical point due to long-range ordering (LRO) at low temperature. Quantum tunneling behavior that transfers from the blocked superparamagnetic (SP) state to the quantum-superparamagnetic (QSP) state was suggested in $CoFe_2O_4$ nanoparticles.[35,36] The state of affairs under which one can observe quantum tunneling of a large magnetic moment between bistable magnetic configurations had been surveyed by Chaudnovsky and Tejada.[37] Hsieh and Lue[35,36] used electron paramagnetic resonance (EPR) to explore the quantum phase transition (QPT) in Fe_3O_4 nanoparticles at low temperatures. Exploration of Cr(II)-doped II−VI materials as a model system for QPT behavior in

Received: September 20, 2011
Published: November 10, 2011

dx.doi.org/10.1021/ja2088426 | J. Am. Chem. Soc. 2012, 134, 2172−2179

DMSQDs has not been reported to date. Further excitement with regard to Cr(II)-doped II−VI QDs exists due to the potential intermediate behavior between Brillouin and van Vleck paramagnetism, as well as a multiply non-denegenate magnetic ground state arising from strong Jahn−Teller (JT) distortion at the Cr(II) dopant site.

The incorporation of intentional defects into a semiconductor host lattice, generated by doping with TM guest ion, produces rational effects on the electronic, optical and magnetic properties of these materials. The elementary interaction of charge, lattice, and magnetic degrees of freedom in quantum-confined systems makes DMSQDs based on CdSe an ideal system to interrogate the physics underlying the QPT, which is quite involved and in many cases is not yet completely understood.[13,38−40] The sp−d exchange behavior will be influenced by QD size, dopant concentration, carrier density, and the site of doping (core vs surface),[41−43] as well as contributions from clustering of ions. In CdSe DMSQDs, additional contributions from surface donor states due to ligation can lead to intrinsic carriers that can enhance the magnetic exchange interactions.[41,42]

In this article, we report the observation of room-temperature FM in Cr(II)-doped CdSe (CdCrSe) QDs prepared by lyothermal methods. The chemically synthesized QDs are 3.1 nm in diameter, doped at 0.6% Cr to form a $Cd_{0.994}Cr_{0.006}Se$ alloy. At a doping level of 0.6%, the Cr(II) ions are stochastically doped with an average content of 2−3 Cr ions per QD. The low concentration of Cr(II) indicates that Cr−Cr magnetic exchange is insignificant and can be described as a p−d exchange-mediated process, as theoretically predicted. A low-temperature critical phase transition is observed at 20 K in the EPR and superconducting quantum interference device (SQUID) measurements. The magnetization transition may reflect ordering of the spin-glass surface or the onset of LRO, reflecting a potential emergence of a quantum superparamagnet. Further studies are underway to interrogate this phenomenon.

2. MATERIALS AND METHODS

Preparation of 0.6% Cr(II):CdSe Quantum Dots. The syntheses of pure CdSe and 0.6% Cr(II)-doped CdSe (CdCrSe) QDs were performed under N_2 using a lyothermal method based on modification of a previously described single-source precursor approach for preparation of doped II−VI QDs.[14,44−49] For the synthesis of pure and doped CdSe, a cluster of $Li_4[Se_4Cd_{10}(SC_6H_5)_{16}]$ (Cd_{10}) was prepared using $Li_4[Cd_4(SC_6H_5)_{10}]$ and pure Se dissolved in acetonitrite. Briefly, 480 mg of Cd_{10} and 21 mg of $CrCl_2$ were dissolved in 20 mL of hexadecylamine and heated to 120 °C for 1 h to initiate metal ion exchange within the cluster. The QDs were grown by increasing the reaction temperature to 220 °C for 6 h. Isolation of QDs was achieved by addition of a minimal amount of toluene followed by addition of methanol to induce particle precipitation. The precipitate was collected via centrifugation and decantation of the supernatant. This process was repeated three times to ensure reagent-free particles, and the precipitate was dried in vacuum at room temperature.

Characterization. Structural analysis and estimation of the QD size were based on powder X-ray diffraction (pXRD), recorded on 10 mg samples using a Rigaku DMAX 300 Ultima 3 powder X-ray diffractometer (using Cu Kα (λ = 1.5418 Å) radiation). The size of the QD was estimated from the Scherrer broadening of the (110), (103), and (112) reflections in pXRD. The QD optical properties were analyzed from absorption spectra obtained using a Varian Cary 50 UV−vis spectrophotometer and photoluminescence (PL) measurements performed using a Varian Cary Eclipse fluorescence spectrophotometer.

Elemental composition analysis for Cr, Cd, and Se was carried out on acid-digested QDs in triplicate using an Oxford Instruments ED_{2000} X-ray fluorescence (XRF) spectrometer with Cu Kα (λ =1.5418 Å) radiation. For a standard XRF analysis, the powdered sample was completely dissolved in 90% HNO_3, heated to remove excess NO_x, and then diluted to ~3 mL with 2% HNO_3 solution. Calibration curves were generated using commercially prepared 1000 ppm elemental standards in 2% HNO_3.

Magnetic measurements of 20−40 mg powdered samples of QDs were performed using a Quantum Design MPMS XL7 SQUID magnetometer. Zero-field-cooled (ZFC) and field-cooled (FC, 200 G) measurements were done to determine dc susceptibility. Field-dependent magnetization ($\mathbf{M}-\mathbf{H}$) data were collected between −7 and +7 T.

High-frequency EPR (HF-EPR) measurements were performed at the National High Magnetic Field Laboratory (NHMFL), Tallahassee, FL. Microwave detection was performed using a low-noise, fast-response InSb hot-electron bolometer (QMC Ltd.). Microwave frequencies in the range of 100−324 GHz were chosen for our experiments to allow for optimal spectral dispersion and sensitivity.[50] For the EPR experiments, all samples were analyzed as powders.

3. RESULTS AND DISCUSSION

Many approaches to producing doped semiconductor QDs have been reported; however, among the most interesting is the use of single-source inorganic clusters[14,44−46,49] in which TM and inorganic clusters undergo lyothermal degradation to yield internally doped crystal lattices. High PL quantum yields, large productive yields, reasonable size distributions, and effective doping make this approach the method of choice for the synthesis for doped nanocrystals. Utilizing the single-source precursor method yields $Cd_{0.994}Cr_{0.006}Se$ QDs (CdCrSe, 0.6% Cr). based on analysis of the Cr-to-Cd ratio by XRF. Although sulfur incorporation can occur due to thiophenol decomposition in the cluster at elevated temperatures (230 °C), maintaining the reactions below 220 °C should result in minimal S incorporation into the QD lattice.[51] The lack of change in metal (Cr+Cd)-to-Se ratios in the XRF as compared to a CdSe grown from a cluster utilizing selenophenol, where no S incorporation is possible, supports the conclusion that S contamination is below detectable limits in the CdCrSe QD. The isolated CdCrSe QDs are spherical with an average diameter of 3.1 ± 0.2 nm (Supporting Information S1a) and 5−6% size dispersity (Supporting Information S1b) based on transmission electron microscopy (TEM) analysis. In Figure 1a, it is demonstrated that the isolated QDs have a wurtzite crystal structure ($P6_3mc$), as shown by the presence of the (110), (103), (112), and (102) reflections at 35°. Scherrer analyses on the pXRD data are in agreement with the TEM images, indicating a high degree of crystallinity with the undoped CdSe QD exhibiting a 3.0 nm diameter, whereas the CdCrSe QD is 3.1 nm. The measured diameter is well below the Bohr exciton radius (5.3 nm) for bulk CdSe;[8] therefore, thus-prepared QDs are in the strong quantum confinement regime. Consistent with the size determination, the absorption spectra in Figure 1b for the CdSe and CdCrSe QDs have a first exciton absorption feature at 541 nm for the ~3 nm CdSe, whereas in CdCrSe first exciton appears at 549 nm, as expected for a wurtzite CdSe QD. The absorption for the Cr ligand field transitions cannot be seen in Figure 1b.

The pXRD data for CdCrSe exhibit a shift to lower 2θ, which can be interpreted as a Vegard law shift due to the smaller size of the Cr ion relative to Cd(II) (Cd(II), 0.109 nm; Cr(II), 0.094 nm; and Cr(III), 0.075 nm). The average lattice parameter shift indicates a change in the lattice parameters for a and c in

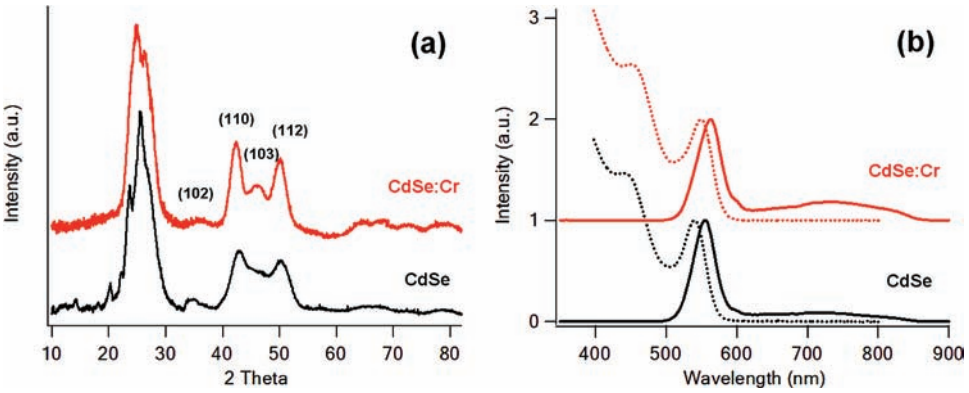

Figure 1. Characterization data for ~3.1 nm (in diameter) 0.6% Cr(II) for CdCrSe QDs: (a) powder X-ray diffraction pattern and (b) room-temperature, solution absorption (dotted), and photoluminescence (solid) spectra for CdCrSe (red) and CdSe (black) QDs.

CdCrSe relative to the undoped CdSe QDs, with a clear elongation along the *c*-direction ($\Delta c/a \approx 1.7\%$). The impact on the average lattice parameter following Cr(II) doping in ZnO has been reported.[52] The observed parameter changes in the pXRD provide strong evidence of Cr doping in the CdSe host matrix.

In Figure 1b, the PL spectra of CdSe and CdCrSe QDs show strong near-band-edge emission at 555 and 563 nm respectively for pure and doped QDs. The shifts in emission from 555 to 563 nm reflect QD size differences.[53−55] In the CdCrSe QDs, the broad emission feature between 600 and 850 nm arises from the defect center recombination in the QDs. There is no evidence of Cr emission in the CdCrSe QDs.[56]

Magnetic Properties. Assigning the oxidation state for the Cr ion dopant in the II−VI lattice is complicated. Chromium is known to replace the cations substitutionally in II−VI QDs, with ion incorporation as Cr(I) $4s^0 3d^5$ or Cr(II) $4s^0 3d^4$ without alteration of the host lattice structure, or as Cr(III) $4s^0 3d^3$ forming the MCr_2Se_4 (M = Cd, Zn) spinel phase.[57] The Cr(II) ion incorporation represents isoelectronic doping onto the tetrahedral Cd(II) site in wurtzite CdSe, resulting in an $S = 2$, $L = 2$ configuration that is prone to JT distortion. Cr(II) has a non-vanishing orbital momentum resulting in intermediate behavior between van Vleck and Brillouin paramagnetism, as well as a mutliplet ground state ($^5T_{2g}$, JT distorted $^5B_{2g}$ ground state).[34] The electronic energy structure of Cr(II) simultaneously with the JT effect has been reported in quite a few papers.[58,59] Spin−orbit (SO) coupling results in further splitting, producing for Se and S lattices two unresolved singlet ground states (Γ_1 and Γ_2), a singlet excited state (Γ_4), and a doublet excited state (Γ_5) (Supporting Information S2). The energy difference is small between the SO split levels resulting orbital mixtures, which can complicate the magnetic behavior. The ground state of Cr(I) is $^6S_{5/2}$ ($S = 5/2$, $L = 0$) with a sixfold spin degeneracy. Under the crystal field of T_d symmetry, the ground state is the $^6A_{1g}$, which can split due to second-order SO terms into a Γ_8 quadruplet and a Γ_7 doublet with very small splittings.[60] Since the Cr(I) center has $L = 0$, it is expected to exhibit $B_{5/2}$ Brillouin paramagnetism that arises from orbital mixing with the valence band of the host in a Fermi density of states, resulting in an acceptor level (X^-) to which the hole is bound. Chromium in the Cr(III) state in the II−VI lattice will form a spinel crystal structure where $S = 3/2$, $L = 3$ and have a ^4F free ion term[61] in the cubic crystal field. The orbital angular momentum term is quenched in Cr(III), generating a singlet $^4A_{2g}$ ground state[61−63] for Cr(III) with T_d site symmetry which is an orbital triplet $^4\Gamma_4$,[64] which results in an orbital singlet $^4\Gamma_2$ with a fourfold spin degeneracy[62] when a JT distortion is combined with spin−orbital coupling. A Cr(III) system will exhibit $B_{3/2}$ Brillouin paramagnetism since the orbital angular momentum is quenched by crystal field. As shown by Tsoi et al. in analogy to V(II) in CdTe, a JT distortion will occur, producing a ground state with a fourfold spin degeneracy.[62] The EPR and magnetization data on the CdCrSe sample can afford important insights into the electronic configuration of the 3d TM ion in the DMS alloy.

In Figure 2a, the field-dependent HF-EPR measured from 100 to 324 GHz is shown at 50 K, plotted relative to $\mathbf{B}-(h\nu/g\beta)$ to center the EPR transition, since the resonance will be frequency dependent. At 100 GHz, three EPR features can be identified. The features are indicated in Figure 2b at 324 GHz. With increasing field, the EPR data show a shift in the resonance and loss of intensity for the broad feature (peak 2) at low field and small changes for the two remaining EPR features (peaks 1 and 3). The increased broadening of the EPR features with increasing field is typical for HF-EPR measurements.[65] The two broad features at $g_{(2)} = 2.075$ and $g_{(3)} = 1.986$ arise from Cr(II) occupying a JT-distorted Cd(II) site in the CdSe host lattice. The *g* values are close to the typical Cr(II) Landé *g*-value, which is around 2.00 and is split by large zero-field splitting (ZFS) term (D). Peaks 2 and 3 in the EPR spectra arise from ZFS due to the large D-term in the spin Hamiltonian, resulting in splitting of the EPR levels into $M_s = 0, \pm1$, and ±2 states. Although four transitions are anticipated in Cr(II), the observed EPR spectrum is consistent with the measured EPR field sweep for Cr(II) in the CdSe lattice,[66] allowing definitive assignment of Cr(II) as the dopant in the lattice. The Landé $g_{(1)} = 1.979$ for peak 1 may arise from Cr(III) impurities, which exhibit a Landé *g*-value of 1.98. Alternately, this peak might reflect the on-setting of ferromagnetism as suggested for materials that exhibit a transition from a blocked SP state to a ferromagnetic single domain at low temperature, reflecting the magnetic polarization of the surface spins which exhibit spin glass behavior.[35,36,67,68] FM in CdCrSe is possible and has been theoretically predicted.[69] Further insight into the potential for a QPT will be gleaned from temperature-dependent EPR and the temperature- and field-dependent magnetization data, as discussed further below.

A plot of the frequency-dependent resonance fields for the three features is shown in Figure 2b. The plots of the field

dx.doi.org/10.1021/ja2088426 |*J. Am. Chem. Soc.* 2012, 134, 2172–2179

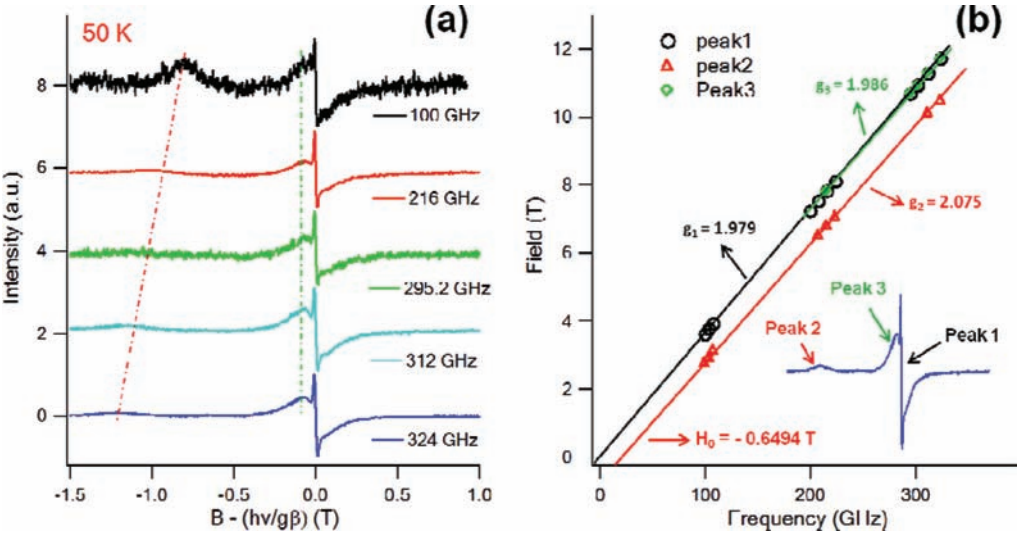

Figure 2. (a) Frequency-dependent EPR spectra of $Cd_{1-x}Cr_xSe$ from 100 to 324 GHz at 50 K for 3.1 nm CdCrSe QDs. (b) Lande *g*-factors fit from frequency-dependent HF-EPR data, yielding $g_{(1)}$ = 1.979 (peak 1), $g_{(2)}$ = 2.075 (peak 2), and $g_{(3)}$ =1.986 (peak 3). Inset shows the 324 GHz EPR data at 50 K.

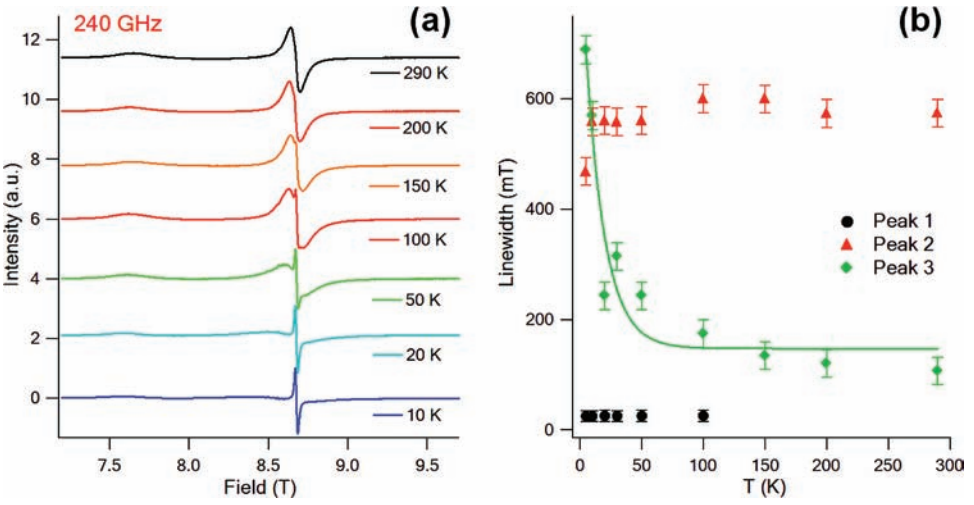

Figure 3. (a) Temperature-dependent HF-EPR spectra (240 GHz) from 10 to 290 K. (b) Plot of line width of the three peaks as a function of temperature.

dependence for peaks 1 and 3 have a zero *y*-intercept. Peak 2 has a nonzero intercept, at $H_0 = -0.6494$ T. The nonzero intercept is due to the presence of the SO split nearly degenerate set of singlets Γ_1, Γ_2, as shown in Supporting Information S2. For a JT-distorted Cr(II), one expects a large ZFS, resulting in an energy level diagram producing a singlet Γ_4 with $m_s = 0$, a doublet Γ_5 with $m_s = \pm 1$, and the two nearly degenerate Γ_1 and Γ_2 singlets with $m_s = \pm 2$, as well as their Zeeman sublevels in the existence of the magnetic field. From the *y*-intercept for peak 2 ($g_{(2)}$ = 2.075) the ZFS of the level can be extracted, yielding a *D*-value of 0.32 cm^{-1}. The observed *D*-value is essentially similar to that for CdCrTe.[70] The nonzero intercept for peak 2 is indicative of a multiplet ground state (Γ_1, Γ_2), while peak 3 arises from the Γ_5 SO split state, yielding a *y*-intercept of zero, consistent with the assignment of a singlet state. The data are consistent with the expectations for JT distortion coupled to SO contributions to the energy levels in the Cr(II) system. For the present case we can conclude that the spectrum is typical of the Cr(II) state in the sample. Consistent with the assignment of the Cr ions being predominately Cr(II), magnetization measurements showed that the majority of Cr ions in Cd sulfides and selenides are in the Cr(II) state.[71−73]

The temperature-dependent (10−290 K) HF-EPR spectra at 240 GHz for the CdCrSe QDs are shown in Figure 3a. For comparison, the HF-EPR data at 324 GHz from 1.5 to 290 K are shown in Supporting Information S3. Although the positions for the EPR transitions do not shift with temperature, a clear transition occurs in the EPR spectra below 290 K, with an increased contribution from the sharp feature (peak 1) and broadening of peaks 2 and 3. A plot of the linewidth of the transition with respect to temperature is shown in Figure 3b. The experimental data exhibit a clear broadening of the EPR feature (peak 3) below 20 K, and no significant change in linewidth for peaks 1 and 2 within experimental error. The line broadening for

dx.doi.org/10.1021/ja2088426 |*J. Am. Chem. Soc.* 2012, 134, 2172–2179

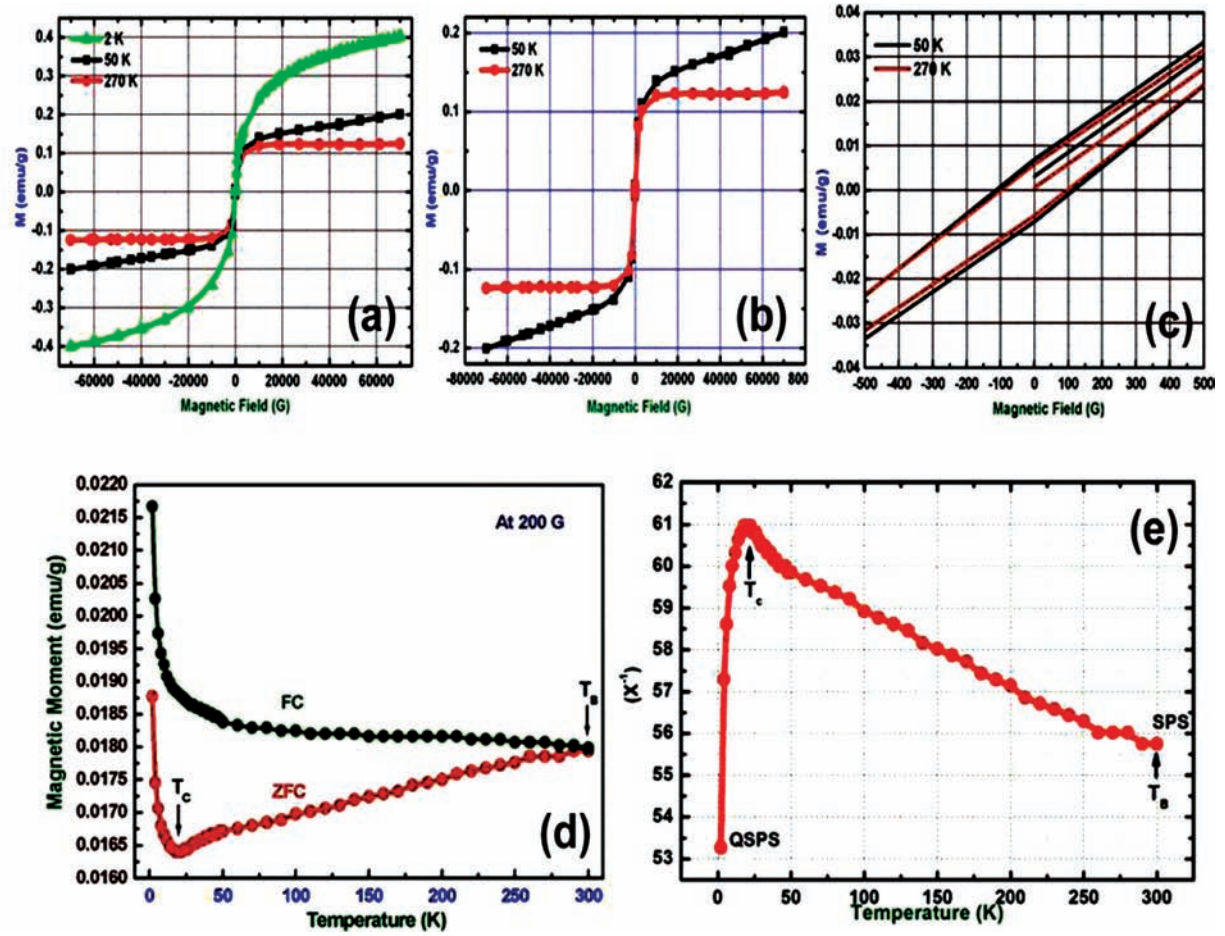

Figure 4. (a) **M**−**H** plot at different temperatures (2, 50, and 270 K) for 3.1 nm CdCrSe between −7 and +7 T. (b) **M**−**H** plot at 50 and 270 K between −7 and +7 T. (c) Hysteresis loop for CdCrSe between −500 and +500 G. (d) Temperature dependence of ZFC/FC magnetization plots measured between 2 and 300 K. The blocking temperature (T_B) and the critical phase transition temperature (T_c) are indicated on the ZFC data set. (e) Variation in inverse magnetization with temperature for the 3.1 nm CdCrSe QDs.

peak 3 fits to an exponential behavior indicative of a change in state population at low T, consistent with the non-degenerate multiplet in Cr(II) samples in CdCrSe. The anomalous line broadening at ∼20 K is indicative of a magnetic phase transition within the sample and has been interpreted as a QPT behavior for ferrous oxides at the nanoscale.[35,36,68]

Further insight into the phase transition requires investigation of the magnetization behavior (**M**−**H**) for the sample. In Figure 4, the field-dependent magnetization is shown as a function of temperature. The sample exhibits SP behavior at room temperature, with M_{sat} = 0.12 emu/g. In Cr(II)-doped II−VI semiconductors, the JT distortion produces an anisotropic lattice wherein the magnetization is dependent on the lattice orientation, making complete interpretation of the M_{sat} value difficult.[73] However, the saturation behavior is consistent with the predictions for ferromagnetic p−d exchange (valence band to t_2 Cr(II) level) in the QDs. The observed spin value is lower than expected due to the negative contribution of L, as previously reported. With decreasing temperature, the magnetization is observed to increase from 0.12 to 0.40 emu/g at 7 T, coupled to a loss of saturation. The increased magnetization at low T may reflect contributions from spin-glass behavior of the surface dopants[35,36] or spin carriers arising from surface ligation, as described previously.[14] Further insight into the magnetization will be discussed in the next section.

Figure 4c displays the zoom region between −500 and 500 G to show more clearly the hysteresis loop for temperatures 50 and 270 K. The coercivity (H_c) at 270 and 50 K is observed to be 100 Oe (Figure 4c). At 50 K the H_c is not observed to change, indicative of a ferromagnetic exchange in the CdCrSe QDs at room temperature. The temperature-dependent FC (200 Oe) and ZFC magnetization data are shown in Figure 4d. ZFC magnetization decreases as the temperature rises from 2 K, reaches a minimum temperature T_c near 20 K, and starts increasing from this point to the blocking temperature T_B at 300 K. The ZFC vs FC data show clear evidence of room-temperature FM with T_B > 300 K. The large difference between ZFC and FC data indicates a large anisotropic field within the QDs. In addition, a phase transition is observed at 20 K with increased magnetization, indicative of long-range magnetic ordering in the CdCrSe QDs. The 20 K phase transition is labeled as a critical phase transition (T_c) and occurs at the transition temperature where the sharp EPR feature becomes dominant (Figure 3b). Within T_B and T_c, the magnetization is proportional to T, while it behaves as $1/T$ below T_c. Further evidence of the critical phase transition at 20 K producing the anomalous

dx.doi.org/10.1021/ja2088426 |*J. Am. Chem. Soc.* 2012, 134, 2172–2179

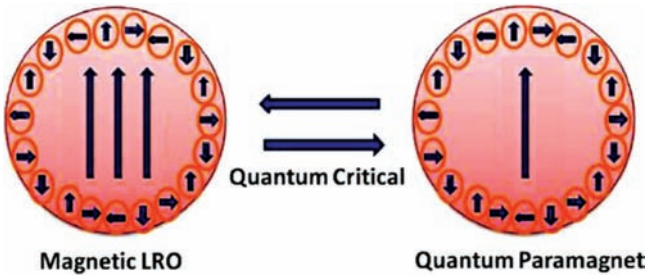

Figure 5. Proposed model of the onset of phase transition in ultrasmall (~3.1 nm in diameter) CdCrSe QDs at low temperature.

magnetization behavior can be observed by inspection of the reciprocal susceptibility χ^{-1} for CdSe:Cr QDs (Figure 4e).

Anomolus Magnetic Behavior. The experimental results show for the first time that lyothermally prepared Cr(II)-doped CdSe QDs exhibit room-temperature FM. Due to the small QD size, SP blocking behavior is observed above 300 K. At a doping level of 0.6%, the number of Cr(II) ions for a 3.1 nm QD is ~2−3. The Cr ions will be stochastic with respect to surface and core sites, and the concentration will represent a stochastic distribution for the QD ensemble. At 0.6%, Cr−Cr exchange interactions are negligible. Theoretical considerations have shown that the t_2 level for the Cr(II) ion lies at the Fermi level, producing ferromagnetic exchange due to p−d exchange coupling with the semiconductor valence band.[69] Magnetic circular dichroism (MCD) experiments on Cr(II)-doped II−VI semiconductors have confirmed the presence of strong p−d exchange leading to ferromagnetic DMS behavior.[34] Recently, MCD in $Zn_{1-x}Cr_xTe$ films (with x = 0.2) revealed the occurrence of room-temperature (300 K) FM.[74,75] Saito et al. demonstrated that $Zn_{1-x}Cr_xTe$ is the third real ferromagnetic DMS after $In_{1-x}Mn_xAs$ and $Ga_{1-x}Mn_xAs$, in which the sp−d exchange interaction could be used to develop spintronic devices.[75,76] Pekarek et al. claimed that even in bulk $Zn_{1-x}Cr_xTe$ with small x (x = 0.0033), due to the low solubility of Cr in ZnTe, and thus inhomogeneities in the crystal, the Cr-rich region exhibits FM with a transition temperature well above room temperature.[77]

Due to orbital angular momentum, the strong p−d exchange in Cr(II)-based DMSQDs leads to ferromagnetic coupling rather than the typical antiferromagnetic (AFM) exchange coupling observed for Mn(II)-doped DMSQDs. The saturation magnetic moment can be ascribed to magnetization of the surface as the temperature is decreased, reflecting the spin-glass behavior of the surface and surface carriers.

Although room-temperature FM is not surprising nor is the increasing M_{sat} with decreasing T, the anomalous magnetization behavior with an observed critical phase transition at 20 K in the EPR and magnetization experiments is surprising. It has been suggested that such non-Curie−Weiss behavior for $T < T_B$ could be attributed to strong dipolar interaction between QDs.[78−84] One possibility for the critical phase transition is a change from a short-range SP behavior at room temperature due to the onset of a ferromagnetic exchange to a LRO as the surface spins magnetize. Such LRO has been reported in ferrites and iron clusters and attributed the observation to a QPT. Consistent with a QPT, a sharp feature (peak 1 in Figure 2) arises in the EPR indicative of a FMR behavior coupled to line broadening of the Cr(II) signature (peak 3 in Figure 2). The correlated phase transition in the EPR and the enhanced magnetization at 20 K in the SQUID, without changes to the coercivity, are indicative of LRO in the powdered QD sample.

As shown in Figure 5, the magnetization behavior can be fit to a simplistic model showing a ferromagnetic single-domain structure below room temperature, followed by LRO at ~20 K, potentially due to the onset of a QPT. The observed anomalous behavior in magnetism of QDs below a certain critical size can be envisioned as a single domain, in contrast to the usual multidomain structure of bulk materials. The SP state for QDs exhibits thermally induced fluctuations in the direction of magnetization.[35−37] The thermal fluctuation of the random spin orientation is blocked ("frozen"), which induces magnetization of the spin-glass surface layer, producing a long-range magnetic order in the QDs. The spin-glass behavior for the surface arises from the larger surface-to-volume ratio in QDs producing an anisotropic field that frustrates the inner spins. The frustration would result in quantum tunneling at low temperatures.[35−37] At low temperatures, the anisotropic energy is larger than the thermal energy, rendering the nanoparticles readily blocked. At even lower temperatures, the anisotropic energy of magnetic nanoparticles enhanced 2−3 orders over the bulk value exhibits QPT from LRO to QSP.[35,68] Such quantum tunneling behavior in a QD has been described but is controversial.[35,36,67,68] Further studies are required to prove the presence of the QPT in the CdCrSe QDs. Further theoretical and experimental studies are needed to understand the observed phenomenon completely.

4. CONCLUSIONS

In summary, we conclude that Cr-doped CdSe quantum dots exhibit room-temperature ferromagnetism with a critical phase transiton to long-range order occurring at 20 K. The ferromagnetic behavior reflects strong p−d exchange based upon theoretical predictions in bulk materials due to formation of a half-metal.[69] The low-temperature phase transition is coupled to magnetic ordering of the surface states that exhibit spin-glass behavior. Consistent with low-temperature long-range ordering, the EPR data exhibit coupled to an enhanced magnetization in the SQUID data. Whether the critical transition represents a transition from a superparamagnetic to a quantum-superparamagnetic state is not clear, but the data are consistent with reports of such behavior at the nanoscale and warrant further investigation.[35,36,68]

■ ASSOCIATED CONTENT

Supporting Information. TEM and size dispersity analysis of $Cd_{0.994}Cr_{0.006}Se$, energy splitting diagram for Cr(II), and temperature-dependent HF-EPR data at 324 GHz. This material is available free of charge via the Internet at http://pubs.acs.org.

■ AUTHOR INFORMATION

Corresponding Author
kedarbhp@rediffmail.com

■ ACKNOWLEDGMENT

We thank NSF-DMR-0701462 for financial support and acknowledge Dr. Johan van Tol for assistance in measuring the HF- EPR at the National High Magnetic Field Laboratory via the NSF Cooperative Agreement No. DMR-0654118 and the State

of Florida. We are very thankful to Prof. K. Sato (Institut fur Festkorperforschung, Forschungszentrum Julich Germany, and Department of Condensed Matter Physics, The Institute of Scientific and Industrial Research, Osaka University, Japan) for fruitful discussion and scientific comments on our results. P.K. is grateful for support from the University Grant Commission, New Delhi, for providing financial assistance under Dr. D. S. Kothari Postdoctoral Fellowship Scheme. K.S. is thankful to the Department of Science and Technology, Government of India, New Delhi, for providing a BOYSCAST Fellowship to carry out this work at Florida State University.

REFERENCES

(1) Murray, C. B.; Norris, D. J.; Bawendi, M. G. *J. Am. Chem. Soc.* **1993**, *115*, 8706–8715.
(2) Li, J. J.; Wang, Y. A.; Guo, W.; Keay, J. C.; Mishima, T. D.; Johnson, M. B.; Peng, X. *J. Am. Chem. Soc.* **2003**, *125*, 12567–12575.
(3) Qu, L.; Peng, X. *J. Am. Chem. Soc.* **2002**, *124*, 2049–2055.
(4) Talapin, D. V.; Rogach, A. L.; Kornowski, A.; Haase, M.; Weller, H. *Nano Lett.* **2001**, *1*, 207–211.
(5) Micic, O. I.; Curtis, C. J.; Jones, K. M.; Sprague, J. R.; Nozik, A. J. *J. Phys. Chem.* **1994**, *98*, 4966–4969.
(6) Guzelian, A. A.; Banin, U.; Kadavanich, A. V.; Peng, X.; Alivisatos, A. P. *Appl. Phys. Lett.* **1996**, *69*, 1432–1434.
(7) Kher, S. S.; Wells, R. L. *Nanostruct. Mater.* **1996**, *7*, 591–603.
(8) Tessler, N.; Medvedev, V.; Kazes, M.; Kan, S. H.; Banin, U. *Science* **2002**, *295*, 1506–1508.
(9) Tan, Z.; Zhang, F.; Zhu, T.; Xu, J.; Wang, A. Y.; Dixon, J. D.; Li, L.; Zhang, Q.; Mohney, S. E.; Ruzyllo, J. *Nano Lett.* **2007**, *7*, 3803–3807.
(10) Bruchez, M.; Moronne, M.; Gin, P.; Weiss, S.; Alivisatos, A. P. *Science* **1998**, *281*, 2013–2016.
(11) Chan, W. C. W.; Nie, S. M. *Science* **1998**, *281*, 2016–2018.
(12) Talapin, D. V.; Poznyak, S. K.; Gaponik, N. P.; Rogach, A. L.; Eychmuller, A. *Phys. E Low-Dimens. Syst. Nanostruct.* **2002**, *14*, 237–241.
(13) Bryan, J. D.; Gamelin, D. R. In *Progress in Inorganic Chemistry*; Karlin, K. D., Ed.; Wiley: New York, 2005; Vol. 54, pp 47−126.
(14) Zheng, W.; Strouse, G. F. *J. Am. Chem. Soc.* **2011**, *133*, 7482–7489.
(15) Hanbicki, A. T.; Jonker, B. T.; Itskos, G.; Kioseoglou, G.; Petrou, A. *Appl. Phys. Lett.* **2002**, *80*, 1240–1242.
(16) Schmidt, G.; Ferrand, D.; Molenkamp, L. W.; Filip, A. T.; van Wees, B. J. *Phys. Rev. B* **2000**, *62*, R4790–R4793.
(17) van Son, P. C.; van Kempen, H.; Wyder, P. *Phys. Rev. Lett.* **1987**, *58*, 2271–2273.
(18) Fiederling, R.; Keim, M.; Reuscher, G.; Ossau, W.; Schmidt, G.; Waag, A.; Molenkamp, L. W. *Nature* **1999**, *402*, 787–790.
(19) Matsumoto, Y.; Murakami, M.; Shono, T.; Hasegawa, T.; Fukumura, T.; Kawasaki, M.; Ahmet, P.; Chikyow, T.; Koshihara, S.; Koinuma, H. *Science* **2001**, *291*, 854–856.
(20) Ogale, S. B.; Choudhary, R. J.; Buban, J. P.; Lofland, S. E.; Shinde, S. R.; Kale, S. N.; Kulkarni, V. N.; Higgins, J.; Lanci, C.; Simpson, J. R.; Browning, N. D.; Das Sarma, S.; Drew, H. D.; Greene, R. L.; Venkatesan, T. *Phys. Rev. Lett.* **2003**, *91*, 077205.
(21) Baik, J. M.; Lee, J. L. *Adv. Mater.* **2005**, *17*, 2745–2748.
(22) Jayakumar, O. D.; Gopalakrishnan, I. K.; Kulshreshtha, S. K. *Adv. Mater.* **2006**, *18*, 1857–1860.
(23) Xing, G. Z.; Yi, J. B.; Tao, J. G.; Liu, T.; Wong, L. M.; Zhang, Z.; Li, G. P.; Wang, S. J.; Ding, J.; Sum, T. C.; Huan, C. H. A.; Wu, T. *Adv. Mater.* **2008**, *20*, 3521–3527.
(24) Klingshirn, C. *Chem. Phys. Chem.* **2007**, *8*, 782–803.
(25) Hong, N. H.; Sakai, J.; Huong, N. T.; Ruyter, A.; Brize, V. *J. Phys.: Condens. Matter* **2006**, *18*, 6897–6905.
(26) Peleckis, G.; Wang, X. L.; Dou, S. X. *Appl. Phys. Lett.* **2006**, *88*, 132507.
(27) Hu, S. J.; Yan, S. S.; Lin, X. L.; Yao, X. X.; Chen, Y. X.; Liu, G. L.; Mei, L. M. *Appl. Phys. Lett.* **2007**, *91*, 262514.
(28) Chu, D. W.; Zeng, Y. P.; Jiang, D. L. *Appl. Phys. Lett.* **2008**, *92*, 182507.
(29) Philip, J.; Punnoose, A.; Kim, B. I.; Reddy, K. M.; Layne, S.; Holmes, J. O.; Satpati, B.; Leclair, P. R.; Santos, T. S.; Moodera, J. S. *Nat. Mater.* **2006**, *5*, 298–304.
(30) Kharel, P.; Sudakar, C.; Sahana, M. B.; Lawes, G.; Suryanarayanan, R.; Naik, R.; Naik, V. M. *J. Appl. Phys.* **2007**, *101*, 09h117.
(31) Bizo, L.; Allix, M.; Niu, H.; Rosseinsky, M. J. *Adv. Funct. Mater.* **2008**, *18*, 777–784.
(32) Xing, P. F.; Chen, Y. X.; Yan, S. S.; Liu, G. L.; Mei, L. M.; Wang, K.; Han, X. D.; Zhang, Z. *Appl. Phys. Lett.* **2008**, *92*, 022513.
(33) Raebiger, H.; Lany, S.; Zunger, A. *Phys. Rev. Lett.* **2008**, *101*, 027203.
(34) Mac, W.; Khoi, N. T.; Twardowski, A.; Gaj, J. A.; Demianiuk, M. *Phys. Rev. Lett.* **1993**, *71*, 2327–2330.
(35) Hsieh, C. T.; Lue, J. T. *Phys. Lett. A* **2002**, *300*, 636–640.
(36) Hsieh, C. T.; Lue, J. T. *Phys. Lett. A* **2003**, *316*, 329–335.
(37) *Macroscopic Quantum Tunneling of the Magnetic Moment*; Chaudnovsky, E. M., Tejada, J., Eds.; Cambridge Univ. Press: Cambridge, 1998.
(38) Erwin, S. C.; Zu, L. J.; Haftel, M. I.; Efros, A. L.; Kennedy, T. A.; Norris, D. J. *Nature* **2005**, *436*, 91–94.
(39) Norris, D. J.; Efros, A. L.; Erwin, S. C. *Science* **2008**, *319*, 1776–1779.
(40) Brus, L. E. *J. Chem. Phys.* **1984**, *80*, 4403–4409.
(41) Meulenberg, R. W.; Lee, J. R. I.; McCall, S. K.; Hanif, K. M.; Haskel, D.; Lang, J. C.; Terminello, L. J.; van Buuren, T. *J. Am. Chem. Soc.* **2009**, *131*, 6888–6889.
(42) Neeleshwar, S.; Chen, C. L.; Tsai, C. B.; Chen, Y. Y.; Chen, C. C.; Shyu, S. G.; Seehra, M. S. *Phys. Rev. B* **2005**, *71*, 201307.
(43) Kittilstved, K. R.; Gamelin, D. R. *J. Am. Chem. Soc.* **2005**, *127*, 5292–5293.
(44) Magana, D.; Perera, S. C.; Harter, A. G.; Dalal, N. S.; Strouse, G. F. *J. Am. Chem. Soc.* **2006**, *128*, 2931–2939.
(45) Hanif, K. M.; Meulenberg, R. W.; Strouse, G. F. *J. Am. Chem. Soc.* **2002**, *124*, 11495–11502.
(46) Meulenberg, R. W.; van Buuren, T.; Hanif, K. M.; Willey, T. M.; Strouse, G. F.; Terminello, L. J. *Nano Lett.* **2004**, *4*, 2277–2285.
(47) Raola, O. E.; Strouse, G. F. *Nano Lett.* **2002**, *2*, 1443–1447.
(48) Kumar, P.; Singh, K. *J. Nanopart. Res.* **2011**, *13*, 1613–1620.
(49) Srivastava, P.; Kumar, P.; Singh, K. *J. Nanopart. Res.* **2011**, *13*, 5077–5085.
(50) Cage, B.; Hassan, A. K.; Pardi, L.; Krzystek, J.; Brunel, L.-C.; Dalal, N. S. *J. Magn. Reson.* **1997**, *124*, 495–498.
(51) Lovingood, D. D.; Oyler, R. E.; Strouse, G. F. *J. Am. Chem. Soc.* **2008**, *130*, 17004–17011.
(52) Xu, C.; Yang, K.; Liu, Y.; Huang, L.; Lee, H.; Cho, J.; Wang, H. *J. Phys. Chem. C* **2008**, *112*, 19236–19241.
(53) Yu, J. G.; Su, Y. R.; Cheng, B. *Adv. Funct. Mater.* **2007**, *17*, 1984–1990.
(54) Yu, J. G.; Li, C.; Liu, S. W. *J. Colloid Interface Sci.* **2008**, *326*, 433–438.
(55) Yu, J. G.; Yue, L.; Liu, S. W.; Huang, B. B.; Zhang, X. Y. *J. Colloid Interface Sci.* **2009**, *334*, 58–64.
(56) Bhaskar, S.; Dobal, P. S.; Rai, B. K.; Katiyar, R. S.; Bist, H. D.; Ndap, J. O.; Burger, A. *J. Appl. Phys.* **1999**, *85*, 439–443.
(57) *Semiconductors and Semimetals*; Furdyna, J. K., Kossut, J., Eds.; Academic: San Diego, 1988; Vol. 25.
(58) Boonman, M. E. J.; Mac, W.; Twardowski, A.; Wittlin, A.; van Bentum, P. J. M.; Maan, J. C.; Demianiuk, M. *Phys. Rev. B* **2000**, *61*, 5358.
(59) Vallin, J. T.; Slack, G. A.; Roberts, S.; Hughes, A. E. *Phys. Rev. B* **1970**, *2*, 4313.
(60) Lambe, J.; Kikuchi, C. *Phys. Rev.* **1960**, *119*, 1256–1260.
(61) Abragam, A.; Bleaney, B. *Electron paramagnetic resonance of transition ions*; Dover Publications: New York, 1986.
(62) Christmann, P.; Kreissl, J.; Hofmann, D. M.; Meyer, B. K.; Schwarz, R.; Benz, K. W. *J. Cryst. Growth* **1996**, *161*, 259–263.
(63) Tsoi, S.; Miotkowski, I.; Rodriguez, S.; Ramdas, A. K.; Alawadhi, H.; Pekarek, T. M. *Phys. Rev. B* **2004**, *69*, No. 035209.

(64) Villeret, M.; Rodriguez, S.; Kartheuser, E. *Phys. Rev. B* **1990**, *41*, 10028–10042.
(65) (a) Zheng, W.; Wang, Z.; Wright, J.; Goundie, B.; Dalal, N. S.; Meulenberg, R. W.; Strouse, G. F. *J. Phys. Chem. C* **2011**, *115*, 23305–23314. (b) Park, K.; Novotny, M. A.; Dalal, N. S.; Hill, S.; Rikvold, P. A. *Phys. Rev. B* **2002**, *65*, article 014426. (c) del Barco, E.; Hernandez, J. M.; Tejada, J.; Biskup, N.; Achey, R.; Rutel, I.; Dalal, N.; Brooks, J. S. *Phys. Rev. B* **2000**, *62*, 3018–3021.
(66) Estle, T. L.; Holton, W. C. *Phys. Rev.* **1966**, *150*, 159.
(67) Gider, S.; Awschalom, D. D.; DiVincenzo, D. P.; Loss, D. *Science* **1996**, *272*, 425–426.
(68) Gider, S.; Awschalom, D. D.; Douglas, T.; Mann, S.; Chaparala, M. *Science* **1995**, *268*, 77–80.
(69) Zhang, C. W.; Yan, S. S.; Wang, P. J.; Zhang, Z. *Comput. Mater. Sci.* **2008**, *43*, 710–714.
(70) Stefaniuk, L.; Bester, M.; Virt, I. S.; Kuzma, M. *Acta Phys. Pol., A* **2005**, *108*, 413–418.
(71) Pekarek, T. M.; Miotkowski, I.; Crooker, B. C. *J. Appl. Phys.* **1996**, *79*, 6436–6438.
(72) Pekarek, T. M.; Luning, J. E.; Miotkowski, I.; Crooker, B. C. *Phys. Rev. B* **1994**, *50*, 16914–16920.
(73) Mac, W.; Twardowski, A.; Eggenkamp, P. J. T.; Swagten, H. J. M.; Shapira, Y.; Demianiuk, M. *Phys. Rev. B* **1994**, *50*, 14144–14154.
(74) Saito, H.; Zayets, V.; Yamagata, S.; Ando, K. *J. Appl. Phys.* **2003**, *93*, 6796–6798.
(75) Saito, H.; Zayets, V.; Yamagata, S.; Ando, K. *Phys. Rev. Lett.* **2003**, *90*, No. 207202.
(76) Wolf, S. A.; Awschalom, D. D.; Buhrman, R. A.; Daughton, J. M.; von Molnar, S.; Roukes, M. L.; Chtchelkanova, A. Y.; Treger, D. M. *Science* **2001**, *294*, 1488–1495.
(77) Pekarek, T. M.; Arenas, D. J.; Crooker, B. C.; Miotkowski, I.; Ramdas, A. K. *J. Appl. Phys.* **2004**, *95*, 7178–7180.
(78) Leslie-Pelecky, D. L.; Rieke, R. D. *Chem. Mater.* **1996**, *8*, 1770–1783.
(79) Wang, H.; Zhang, F.; Zhang, W.; Wang, X.; Lu, Z.; Qian, Z.; Sui, Y.; Dong, D.; Su, W. *J. Cryst. Growth* **2006**, *293*, 169–174.
(80) Hou, Y.; Yu, J.; Gao, S. *J. Mater. Chem.* **2003**, *13*, 1983–1987.
(81) García-Otero, J.; Porto, M.; Rivas, J.; Bunde, A. *Phys. Rev. Lett.* **2000**, *84*, 167–170.
(82) Chantrell, R. W.; Walmsley, N.; Gore, J.; Maylin, M. *Phys. Rev. B* **2000**, *63*, 024410.
(83) Mamiya, H.; Nakatani, I.; Furubayashi, T. *Phys. Rev. Lett.* **1998**, *80*, 177–180.
(84) Seehra, M. S.; Babu, V. S.; Manivannan, A.; Lynn, J. W. *Phys. Rev. B* **2000**, *61*, 3513–3518.

■ NOTE ADDED AFTER ASAP PUBLICATION

This article was published ASAP on December 28, 2011, before all author corrections were applied. The corrected version was posted on January 5, 2012.